HHS Public Access

Author manuscript

Mitochondrion. Author manuscript; available in PMC 2020 July 01.

Published in final edited form as:

Mitochondrion. 2019 July ; 47: 282–293. doi:10.1016/j.mito.2019.01.003.

Withaferin A-mediated apoptosis in breast cancer cells is associated with alterations in mitochondrial dynamics

Anuradha Sehrawat[a], **Suman K. Samanta**[a,b], **Eun-Ryeong Hahm**[a], **Claudette St. Croix**[c], **Simon Watkins**[d,e], and **Shivendra V. Singh**[a,e,*]

[a]Department of Pharmacology & Chemical Biology, University of Pittsburgh School of Medicine, Pittsburgh, PA, USA

[b]Institute of Advance Study in Science and Technology, Guwahati, India

[c]Department of Environmental and Occupational Health, University of Pittsburgh, Pittsburgh, PA, USA

[d]Department of Cell Biology and Physiology, University of Pittsburgh School of Medicine, Pittsburgh, PA, USA

[e]UPMC Hillman Cancer Center, Pittsburgh, PA, USA

Abstract

Withaferin A (WA), a steroidal lactone derived from a medicinal plant (*Withania somnifera*), inhibits cancer development in transgenic and chemically-induced rodent models of breast cancer but the underlying mechanism is not fully grasped. We have shown previously that WA treatment causes apoptotic cell death in human breast cancer cells that is preceded by inhibition of complex III of the mitochondrial electron transport chain. This study extends these observations to now demonstrate alterations in mitochondrial dynamics in WA-induced apoptosis. Assembly of complex III was decreased in MCF-7 and SUM159 cells but not in MDA-MB-231 as determined by native blue gel electrophoresis. Because WA is a Michael acceptor (electrophile), we explored the possibility of whether it covalently modifies cysteine residue(s) in ubiquinol-cytochrome *c* reductase, Rieske iron-sulfur polypeptide 1 (UQCRFS1). Covalent modification of cysteine in UQCRFS1 was not observed after WA treatment. Instead, WA treatment inhibited chemically-induced mitochondrial fusion and decreased the mitochondrial volume, and this effect was accompanied by a decrease in the expression of proteins involved in fusion process, including mitofusin1, mitofusin2, and full-length optic atrophy protein 1 (OPA1). A loss of volume in fragmented mitochondria also occurred in WA-exposed cells when compared to vehicle-treated control. WA treatment also caused a decrease in protein level of mitochondrial fission-regulating protein dynamin-related protein 1 (DRP1). Functional studies revealed that *DRP1* deficiency and *OPA1* knockdown attenuated apoptotic potential of WA. Taken together, these results indicate that

*Corresponding author at: 2.32A UPMC Hillman Cancer Center Research Pavilion, 5117 Centre Avenue, Pittsburgh, PA 15213, USA. singhs@upmc.edu.

WA not only alters Complex III assembly but also inhibits mitochondrial dynamics in breast cancer cells.

Keywords

withaferin A; mitochondrial dynamics; apoptosis; breast cancer; chemoprevention

1. Introduction

Withania somnifera, also known as Ashwagandha, is a medicinal plant native to India and neighboring countries, and exhibits diverse pharmacological properties including immunomodulatory, cardiovascular protection, anti-stress, anti-inflammatory, antibiotic, anti-convulsant, hypolipidemic, anti-tumor activities (Mirjalili et al., 2009; Palliyaguru et al., 2016). Due to its broad-spectrum pharmacological effects, root or leaf extract of *Withania somnifera* has been used to alleviate many ailments for thousands of years (Mirjalili et al., 2009; Palliyaguru et al., 2016; Jaradat et al., 2016). Recent studies have also established clinical safety of *Withania somnifera* extract administration in humans (Chandrasekhar et al., 2012; Ambiye et al., 2013; Sharma et al., 2018). Bioactivity of *Withcmia somnifera* is attributed to withanolides or steroidal lactones (Mirjalili et al., 2009; Zhang et al., 2012; Palliyaguru et al., 2016). Among many naturally-occurring withanolides present in root or leaf of *Withania somnifera*, withaferin A (WA) is most effective anticancer agent (Antony et al., 2014; Gu et al., 2014). Anticancer effect of WA has been studied in different cancer types including breast cancer that remains a health concern for women globally (Vyas and Singh, 2014; Chirumamilla et al., 2017).

Our laboratory was the first to determine the efficacy of WA for prevention of breast cancer (Hahm et al., 2013; Samanta et al., 2016), which is still a major health concern for women globally (Siegel et al., 2018). In a mouse model of epidermal growth factor receptor 2-driven estrogen-receptor negative breast cancer, intraperitoneal administration of 100 μg WA (about 4 mg/kg; three times per week for 28 weeks) significantly inhibited tumor burden (palpable tumor weight) and area of microscopic papillary tumors + ductal carcinoma *in situ* and invasive carcinoma while the overall incidence of cancer was not affected significantly (Hahm et al., 2013). Because WA was shown to inhibit estrogen receptor-α (Hahm et al., 2011a), we also determined the efficacy of WA for prevention of estrogen receptor-positive breast cancer using a rat model of chemically-induced cancer (Samanta et al., 2016). In this study, breast cancer incidence was significantly lower in the WA treatment groups (4 mg/kg and 8 mg/kg body weight, 5 times per week intraperitoneally for 10 weeks) compared with control rats (Samanta et al., 2016). Nevertheless, in both studies breast cancer prevention by WA was associated with a significant increase in apoptotic cell death in comparison with respective control tumors (Hahm et al., 2013; Samanta et al., 2016). We also demonstrated that WA was bioavailable in mammary tumor tissues of the rats (Samanta et al., 2016).

Cancer preventive mechanisms of WA, including apoptosis induction, have been studied using human breast cancer cells. Noticeable mechanisms potentially contributing to breast cancer prevention by WA include mitotic arrest (Antony et al., 2014), apoptosis induction

(Hahm et al., 2011b; Hahm et al., 2014), inhibition of epithelial to mesenchymal transition and cell migration (Lee et al., 2010; Lee et al., 2015), and suppression of self-renewal of breast cancer stem-like cells (Kim and Singh, 2014). Apoptosis induction by WA in breast cancer cells was associated with mitochondria-derived reactive oxygen species resulting from inhibition of complex III of the electron transport chain. Because apoptotic response to different stimuli, including certain naturally occurring phytochemicals is regulated by mitochondrial dynamics (Suen et al., 2008; Sehrawat et al., 2017), the present study was undertaken to determine if WA alters mitochondrial fusion and/or fission in breast cancer cells.

2. Materials and Methods

2.1. Reagents

Withaferin A (WA, purity > 95%) was bought from ChromaDex (Irvine, CA) and dissolved in dimethyl sulfoxide (DMSO). Working solution of WA was diluted with complete media immediately before use and concentration of DMSO did not exceed 0.1%. Tissue culture medium was from MediaTech (Manassas, VA) and fetal bovine serum was from Atlanta Biologicals (Flowery Branch, GA). Antibiotics, NativePAGE™ cathode and anode buffers, NativePAGE™ 5% G-250 sample additive, NativePAGE™ running buffer, and NativePAGE™ 3-12% Bis-Tris protein gel were from Invitrogen-Life Technologies (Carlsbad, CA). Mitochondria isolation kit was from ThermoFisher Scientific (Waltham, MA). Digitonin and DMSO were from Sigma-Aldrich (now Millipore-Sigma, St. Louis, MO). Recombinant glutathione S-transferase-tagged ubiquinol-cytochrome *c* reductase, Rieske iron-sulfur polypeptide 1 (RISP or UQCRFS1) protein was purchased from MyBioSource (San Diego, CA). Sources of the antibodies were as follows: anti-mitochondrial dynamin like GTPase (DRP1), anti-phospho-(S637)-DRPl, and anti-mitofusin2 (MFN2) antibodies were from Cell Signaling Technology (Danvers, MA); anti-mitofusinl (MFN1) and anti-fission, mitochondrial 1 (FIS1) antibodies were from Santa Cruz Biotechnology (Dallas, TX); anti-optic atrophy protein 1 (OPA1) antibody was from BD Biosciences (San Jose, CA); anti-β-Actin antibody was from Sigma-Aldrich (St. Louis, MO). FITC-Annexin V/propidium iodide Apoptosis Detection kit was purchased from BD Biosciences. Polyethylene glycol (PEG) 1500 was purchased from Roche Life Sciences (Indianapolis, IN). pAc-green fluorescent protein (GFP)-Mito (mito-GFP) and pDsRed2-Mito (mito-DsRed2) plasmids were kindly provided by Dr. Bennett Van Houten (University of Pittsburgh, Pittsburgh, PA). Human OPA1 siRNA was from Santa Cruz Biotechnology and control siRNA was from Qiagen (Germantown, MD).

2.2. Cell lines

The MDA-MB-231 and MCF-7 cell lines were purchased from the American Type Culture Collection (Manassas, VA) whereas SUM159 cell line was procured from Asterand Bioscience (Detroit, MI). Each cell line was last authenticated by us in March of 2017, and cultured according to the supplier's recommendations. MDA-MB-231 and MCF-7 cells stably transfected with mito-GFP or mito-DsRed2 were cultured in medium supplemented with 100 μg/mL G418. Mouse embryonic fibroblasts (MEF) from wild-type (DRP1+/+) and DRP1 deficient (DRP−/−)mice were a generous gift from Dr. Katsuyoshi Mihara (Kyushu

University, Fukuoka, Japan) and cultured in Dulbecco's modified essential medium supplemented with 10% fetal bovine serum and antibiotics.

2.3. Blue native polyacrylamide gel electrophoresis (BN-PAGE)

The cells (5×10^6 cells in 145-mm dish) were exposed to DMSO (control) or WA for 24 hours and mitochondria were isolated using Mitochondria isolation kit and then solubilized in cold 1 × NativePAGE™ sample buffer containing 5% digitonin. Prior to electrophoresis, 0.5 μL of NativePAGE™ 5% G-250 sample additive was added to 20 μg of mitochondrial protein sample. The upper buffer chamber of electrophoresis equipment was filled with cathode buffer and lower chamber was filled with the anode buffer. Exact volume of protein was loaded in NativePAGE™ 3-12% Bis-Tris protein gel and the voltage was set at 150V. Electrophoresis was performed for about 2 hours. The gels were placed in 100 mL of fix solution (40% methanol/10% acetic acid) and microwaved on high power for 45 seconds. After 15 minutes of shaking, the gel was placed in 100 mL of de-staining solution (8% acetic acid) and microwaved on high power for 45 seconds. The gel was placed on the shaker until the desired background was obtained.

2.4. Mass spectrometry

One μg of recombinant glutathione S-transferase-tagged ubiquinol-cytochrome *c* reductase, Rieske iron-sulfur polypeptide 1 (UQCRFS1) protein was incubated with 16 μM WA for different lengths of time (0, 4, 8, 16, and 24 hours; n=5). Chymotrypsin was used to digest UQCRFS1 overnight at 37°C. Reaction was quenched with 0.1% trifluoroacetic acid and the resultant proteolytic peptides were desalted with PepClean C-18 Spin Columns (Pierce, Rockforn, IL) prior to LC-MS/MS analysis. Samples were analyzed by nano LC-MS/MS with a Waters NanoAcquity HPLC system interfaced to a high-resolution mass spectrometer (LTQ-Orbitrap Velos; ThermoFisher Scientific). The separation was performed on an analytical C18 column (PicoChip™ Reprosil C18, New Objective, Inc., Woburn, MA) using a binary reverse-phase gradient at a flow rate of 300 nL/min. The mass spectrometer was operated in a data-dependent mode, with high-resolution full MS spectra performed in Orbitrap at 60000 FWHM resolution, and data-dependent acquisition was used to collect tandem mass spectra for the 13 most abundant ions detected in the full scan spectra. Protein identification was performed by database matching. Briefly, MS/MS spectra were searched with the MASCOT search engine (Version 2.4.0, Matrix Science) against a UniProt mouse proteome database from the European Bioinformatics Institute (http://www.ebi.ac.uk/integr8) using the following parameters. The mass tolerance was set at 20 *ppm* (parts per million) for the precursor ions and 0.8 Da for the fragment ions. Two mis-cleavages were allowed for trypsin digestion. Dehydro, withaferin A modification of cysteine residues, and oxidation of methionine residues were set as variable modifications. Mass spectrometry data collected for each sample was analyzed using custom dMS software implemented on Chorus (dMS 1.0, University of Pittsburgh and InfoClinika). Briefly, the high-resolution full MS spectra were aligned and the *m/z*, charge state, retention time and intensity data for all molecular features detected in the full scan mass spectra were integrated and matched to protein identification results. Data analysis was performed within CHORUS, a cloud computing data analysis suite developed by the Yates lab (https://chorusproject.org/).

2.5. Polyethylene glycol (PEG)-induced mitochondrial fusion

Cells (1×10^5) stably transfected with mito-GFP were co-plated with the same number of mito-DsRed2 expressing MDA-MB-231 or MCF-7 cells on glass coverslips in 12-well plates. Cycloheximide (20 μg/mL) was added 30 minutes before and kept in all incubations to inhibit *de novo* synthesis of proteins. Cells were then washed with serum-free medium and incubated with pre-warmed solution of PEG 1500 (50% weight/volume) for 1 minute at room temperature. After extensive washing with medium containing 10% serum, cells were treated with DMSO or desired doses of WA for specified time periods. Next, the cells were fixed for 30 minutes with ice-cold 4% formaldehyde in phosphate-buffered saline (PBS), stained with 4',6-diamidino-2-phenylindole (DAPI), and mounted onto glass slides. Randomly selected fields were observed using confocal fluorescence microscope from which the percentage of co-localized fluorescence was calculated using Nikon (NIS) Elements software and expressed as the percentage of mitochondrial fusion as described previously (Sehrawat et al., 2016).

2.6. Confocal microscopy

For determination of mitochondrial volume/fragmentation changes, mito-DsRed2 expressing MDA-MB-231 or MCF-7 cells were cultured on MatTek dishes (MatTek, Ashland, MA), allowed to attach, and then treated with DMSO or desired doses of WA for 3, 6, or 12 hours. After washing with PBS, cells were fixed with 4% paraformaldehyde for 20 minutes, and nuclear DNA was stained with DAPI. Three dimensional stacks of mitochondria at randomly selected fields were collected as a Z-series using an inverted confocal microscope (Nikon Al, Nikon) controlled by NIS-Elements software at 60× objective magnification. A step size of 0.15-0.2 micron was used for the Z-stacks. Images were deconvoluted using the 3D Landweber deconvolution capabilities of Nikon Elements. Deconvoluted images were imported into Imaris (Bitplane Company, Zurich, Switzerland) and the mitochondrial volume, surface area, and sphericity parameter for small mitochondrial fragments, with an arbitrary threshold of sphericity < 0.4 for fragmented mitochondria were calculated. For each cell line, sufficient images were taken to ensure that there were ~30-100 usable individual cells in 5-11 fields per slide for follow-up analysis.

2.7. Determination of apoptosis

Apoptosis was quantified by flow cytometry using FITC-Annexin V/propidium iodide by following the manufacturer's instructions. Briefly, after treatment with DMSO or various doses of WA, the cells were harvested by trypsin treatment and washed with PBS. Cells were resuspended in 100 μL of binding buffer and stained in dark with 4 μL of FITC-Annexin V and 2 μL of propidium iodide solution for 30 minutes at room temperature. Samples were then diluted with 100-200 μL of binding buffer, and stained cells were analyzed using a BD Accuri™ C6 flow cytometer.

2.8. Immunoblotting

Control- and WA-treated cells were processed for immunoblotting as described by us previously (Xiao et al., 2003). Blots were stripped and re-probed with anti-β-Actin antibody

to correct for protein loading differences. Densitometric quantitation was done using UN-SCAN-IT software version 5.1 (Silk Scientific Corporation, Orem, UT).

2.8. Small interfering RNA-mediated knockdown of OPA1

MDA-MB-231 cells (1×10^5 cells per well) were plated in 6-well plates in triplicate, allowed to attach overnight, and then transfected with 100 nM control siRNA or 100 nM human siRNA targeting OPA1 using Oligofectamine™ transfection reagent (Invitrogen-Life Technologies) following manufacturer's recommendations. After 24 hours of transfection, the cells were treated with DMSO or desired concentrations of WA for 12 hours and then processed for immunoblotting or apoptosis assay.

2.9. Statistical analysis

Statistical evaluation was performed using GraphPad Prism software (version 7.02). One-way analysis of variance (ANOVA) followed by Dunnett's test or Bonferroni's test was employed for dose-response comparisons and multiple comparisons, respectively.

3. Results

3.1. Effect of WA treatment on complex III assembly

We have shown previously that WA treatment inhibits complex III activity in breast cancer cells *in vitro* and *in vivo* (Hahm et al., 2011b; Hahm et al., 2013; Samanta et al., 2016). We explored the possibility of whether WA treatment alters complex III assembly. We tested this possibility by blue native gel electrophoresis, and the results are shown in Fig. 1A. A decrease in level of complex III was observed after 24-hour treatment of MCF-7 and SUM159 cells with 2 μM WA in comparison with solvent-treated control, but this effect was not evident in the MDA-MB-231 cell line (Fig. 1B). It is important to point out that the 2 μM WA concentration is achievable in plasma based on a pharmacokinetic study in mice (Thaiparambil et al., 2011). These results indicated cell line-specific decrease in complex III assembly following WA treatment.

3.2. Mass spectrometry to determine potential modification of UQCRFS1 cysteine(s) by WA

Complex III exists as a tightly bound symmetrical dimer, and each monomer is composed by three catalytic subunits (MT-CYB, CYC1, and UQCRFS1), and seven other subunits (Signes and Fernandez-Vizarra, 2018). Assembly of complex III begins with synthesis of MT-CYB but its maturation occurs after addition of the UQCRFS1 and insertion of UQCR11 to the dimeric pre-complex III (Signes and Fernandez-Vizarra, 2018). Because WA is a Michael acceptor (electrophile) and capable of reacting with the sulfhydryl of cysteine residue, we considered the possibility of covalent modification of cysteine residue(s) in UQCRFS1. We have shown previously that mitotic arrest in breast cancer cells following WA exposure is associated with covalent modification of cysteine-303 of β-tubulin (Antony et al., 2014). We tested this possibility by using recombinant glutathione S-transferase-tagged UQCRFS1. Human UQCRFS1 protein has 5 cysteine residues at positions 77, 217, 222, 236, 238, but the recombinant protein used in this study was truncated (amino acid residues 1-78 were lacking). The glutathione S-transferase that was tagged to UQCRFS1 contained 4 cysteine

residues at positions 85, 138, 169, and 178. No evidence for the presence of WA modification on UQCRFS1 was found by differential mass spectrometry analyses of WA-treated samples. A total of 470208 molecular features were detected and quantified by LC-MS/MS. Selected features with significant positive correlation with the length of WA treatment were subjected to targeted identification. MASCOT database search of all tandem mass spectra resulted in identification of two WA modified cysteine residues, both located at the glutathione S-transferase proportion of the recombinant protein at positions 169 and 178 (Fig. 1C, D). These results indicated that WA was unable to modify cysteine residues in UQCRFS1 but this possibility for the cysteine residue at position 77 of UQCRFS1 cannot be fully discarded.

3.3. WA treatment inhibited PEG-induced mitochondrial fusion in human breast cancer cells

Because of published role of mitochondrial dynamics in regulation of apoptosis (Brooks and Dong, 2007; Suen et al., 2008; Grandemange et al., 2009; Boland et al., 2013), we determined the effect of WA treatment on mitochondrial fusion in co-plated human breast cancer cells expressing mito-GFP or mito-DsRed2 which can be visualized in mitochondria with green and red fluorescence, respectively. Because both SUM159 and MDA-MB-231 are estrogen receptor negative unlike MCF-7 cells, only MDA-MB-231 and MCF-7 were used for these studies. As shown in Fig. 2A and 2B, PEG-mediated mitochondrial fusion in DMSO-treated control cells was visible as a yellow fluorescence due to merging of green and red fluorescence. WA treatment decreased the PEG-induced mitochondrial fusion capacity in both MDA-MB-231 and MCF-7 cells (Fig. 2C, D). MCF-7 cells were slightly more sensitive to inhibition of PEG-induced mitochondrial fusion capacity by WA treatment compared with MDA-MB-231 cells. Inhibition of PEG-induced mitochondrial fusion was rapid and evident as early as 3 hours following WA treatment (Fig. 2C, D). These results demonstrated inhibition of mitochondrial fusion ability by WA treatment in both MDA-MB-231 (estrogen-independent) and MCF-7 (estrogen-responsive) cells.

3.4. WA treatment caused a loss in mitochondrial volume in human breast cancer cells

Next, we tested the possibility of whether WA treatment could alter mitochondrial network integrity using mito-DsRed2 expressing MDA-MB-231 and MCF-7 cells. Enlarged images in Fig. 3A displayed time- and dose-dependent morphological alteration of mitochondria upon WA treatment in MDA-MB-231 cells. Percentage of total mitochondrial volume per cell (Fig. 3B), fragmented mitochondrial volume per cell (Fig. 3C), non-fragmented mitochondrial volume per cell (Fig. 3D), and ratio of the fragmented versus non-fragmented mitochondrial volume per cell (Fig. 3E) compared with corresponding DMSO-treated control cells was quantified. Quantification indicated that WA treatment decreased not only volume of total mitochondria but also fragmented mitochondria suggesting inhibition of both mitochondrial fusion and fission. Mitochondrial volume changes with similar trend were also observed in MCF-7 cells after WA treatment (Fig. 4A-E). These results confirm the inhibitory effect of WA on mitochondrial network integrity in human breast cancer cells irrespective of hormone dependency.

3.5. Effect of WA treatment on levels of proteins involved in mitochondrial fusion and fission

As can be seen in Figure 5A, WA-induced apoptosis was evident at 6- and 12-hours of treatment with WA, and the effect was statistically significant at the 4 μM concentration in both cell lines. DRP1 is a key regulator of mitochondrial fission and its phosphorylation modulates its activity (Cereghetti et al., 2008; Cho et al., 2013). Studies have shown that calcineurin-dependent dephosphorylation of DRP1 regulates its translocation to mitochondria (Cereghetti et al., 2008). In fused condition, DRP1 is sequestered in the cytoplasm upon its phosphorylation (Corrado et al., 2012). Upon dephosphorylation, DRP1 is recruited to the outer mitochondrial membrane for oligomerization and interaction with other fission-related proteins including FIS1 (Corrado et al., 2012). WA treatment caused an increase in phospho-(S637)-DRPl in both MDA-MB-231 (Fig. 5B) and MCF-7 cells (Fig. 5C). Moreover, the DRP1 level was decreased in cells treated with WA compared with respective controls in both cell lines (Fig. 5B, C). Interestingly, response of another fission-associated protein FIS1 expression exposed to WA treatment was not quite the same as DRP1 in both cell lines (Fig. 5B, C). These results suggested that the inhibition of mitochondrial fission by WA treatment may be DRP1-dependent.

Next, we examined the expression mitochondrial fusion regulating proteins MFN1, MFN2, and OPA1 (OPA1-L and OPA1-S). Fig. 5B and 5C show that expression of these proteins except OPA1-S were downregulated by WA treatment in both cells. However, OPA1-S expression was increased in WA-treated cells when compared with respective controls. Long, membrane-bound form of OPA1, which is located at the inner mitochondrial membrane, is necessary for mitochondrial fusion, but its processing to short-soluble forms inhibits fusion and can facilitate mitochondrial fission (MacVicar and Langer, 2016). Increased processing of OPA1 facilitates fragmentation of mitochondria and eventually triggers cell death (MacVicar and Langer, 2016). These results demonstrated that WA-induced apoptosis was associated with downregulation of DRP1, MFN1, MFN2, and OPA1-L but an increase in OPA1-S form.

3.6. DRP1 knockout attenuated WA-induced apoptosis

Proapoptotic or anti-apoptotic role of DRP1 in cancer is still controversial and depends on the type of tumor (Estaquier and Arnoult D, 2007; Cassidy-Stone et al., 2008; Inoue-Yamauchi and Oda, 2012; Rehman et al., 2012; Lima et al., 2018). However, recent study showed that DRP1 expression was positively proportionally correlated with breast cancer degrees suggesting DRP1 could be an effective therapeutic target for breast cancer treatment (Zhao et al., 2013). This report encouraged us to further determine the role of DRP1 in WA-mediated apoptosis. Wild-type and DRP1-deficient MEF cells were utilized to test this question. Depletion of DRP1 expression was confirmed in DRP1−/− MEF. WA treatment decreased the expression level of DRP1 protein in wild-type DRP1+/+ MEF (Fig. 6A). DRP1 deficiency alone caused a significant increase in apoptosis (>3-fold increase) compared with wild-type DRP1+/+ MEF. When the data for WA-treated groups was computed compared to respective DMSO-treated control, it was clear that WA-induced apoptosis was attenuated in DRP1−/− MEF compared to DRP1+/+ cells (Fig. 6B). These results suggested that while DRP1 deficiency alone potentiated apoptosis, the cell death

resulting from WA treatment was attenuated in these cells in comparison with DRP1+/+ MEF (Fig. 6B).

3.7. OPA1 knockdown attenuated WA-mediated apoptosis

Many studies evidenced the influence of OPA1 loss on apoptosis regulation (Olichon et al., 2003; Lee et al., 2004; Arnoult et al., 2005). Unlike other mitochondrial fusion proteins, OPA1 localizes in mitochondrial inner membrane and regulates not only mitochondrial fusion but also maintenance of cristae structure which is rich in cytochrome *c*. Downregulation of OPA1 could disrupt normal cristae structure, thus releasing sequestered cytochrome *c*, and subsequently accelerate apoptosis. To investigate whether OPA1 could affect WA-mediated apoptosis in breast cancer cells, MDA-MB-231 cells were transiently transfected with a control siRNA or OPA1-targeted siRNA. OPA1-L expression was completely abolished by its knockdown as can be seen in Fig. 6C. WA-mediated increase in OPA-S form was also markedly suppressed in cells transiently transfected with OPA1-targeted siRNA (Fig. 6C). Fig. 6D shows flow histograms for Annexin V and propidium iodide staining following treatment with DMSO (control) or WA in MDA-MB-231 cells transfected with a control siRNA or OPA1-targeted siRNA. Like results in cells with DRP1 deficiency (Fig. 6B), OPA1 knockdown attenuated WA-induced apoptosis especially at the higher concentration when the results were normalized for the respective DMSO-treated controls (Fig. 6E). These results indicated a partial role for OPA1 in regulation of WA-induced apoptosis.

4. Discussion

Present study was inspired by our previous work with benzyl isothiocyanate, which is another naturally-occurring cancer chemopreventative phytochemical present in edible cruciferous vegetables like garden cress, on dysregulation of mitochondrial dynamics as WA shares many features with this agent in breast cancer (Sehrawat et al., 2017). WA treatment downregulated both mitochondrial fusion and fission in association with the inhibition of PEG-induced mitochondrial fusion, increase in loss of mitochondrial volume, and suppression of proteins related to this process. Inhibition of both mitochondrial fusion and fission by microtubule inhibitor nocodazole has been documented (Woods et al., 2016). Because mitochondria travel along microtubules, disruption of microtubules could impair mitochondrial movement, subsequently mitochondria become arrested. Because WA binds to β-tubulin and disorganizes network of microtubules (Antony et al., 2014), inhibition of mitochondrial dynamics may be associated with downregulation of β-tubulin at least in breast cancer cells.

Activity of fission protein DRP1 as well as its expression was decreased in WA-treated cells compared with control. Post-translational modification including phosphorylation modulates DRP1 activity positively or negatively depending on kinases (Cereghetti et al., 2008; Cho et al., 2013). Phosphorylated DRP1 at S616 residue by Cdk1 promotes mitochondrial fission (Cereghetti et al., 2008; Cho et al., 2013) and this phosphorylation was found to be inhibited in WA-treated cells in present study (data not shown). Previously we have shown that WA treatment decreased Cdk1 expression in both MDA-MB-231 and MCF-7 cells (Stan et al.,

2008). Therefore, the suppression of DRP1 activity in WA-treated cells could be due to Cdk1 downregulation.

Maycotte et al. (2017) reviewed the alteration of proteins associated with mitochondrial dynamics in diverse tumor samples. Upregulation of DRP1 fission regulating protein was found in many type of tumors such as liver, lung, prostate, breast, and pancreas indicating its implication in cancer progression (Maycotte et al., 2017). On the other hand, expression of fusion proteins MFN1 and MFN2 were decreased in liver and lung tumors compared with peritumor area or normal tissue, respectively (Maycotte et al., 2017). Therefore, DRP1 may be an effective therapeutic target for the treatment of cancer including breast tumor. WA treatment downregulated DRP1 expression in both breast cancer cells and its deficiency partially attenuated apoptosis in WA-treated cells suggesting a role for DRP1 in WA-mediated apoptosis.

WA treatment decreased OPA1-L expression concomitant with increased expression of OPA1-S in both breast cancer cells. OPA1 undergoes proteolytic cleavage by a protease OMA1 (Jiang et al., 2014; Pham et al., 2016). During apoptosis, Bak and Bax oligomerization activates OMA1 to cleave OPA1-L and thus cleaved OPA1-L (OPA1-S) triggers apoptosis *via* cristae remodeling leading to cytochrome *c* release (Jiang et al., 2014; Pham et al., 2016). Bak is reported to be essential for WA-mediated apoptosis in breast cancer cells by us (Hahm et al., 2011b). The results of the present study are perplexing because RNA interference of OPA1 prevented WA-induced apoptosis. Further work is necessary to resolve this discrepancy. In conclusion, the present study reveals that WA-mediated apoptosis is associated with dysregulation of mitochondrial dynamics in breast cancer cells.

Acknowledgements

This work was supported by the grant ROI CA142604 awarded by the National Cancer Institute (S. V. Singh). This study used the Cancer Proteomics Facility, the Cell and Tissue Imaging Facility, and the Flow Cytometry Facility supported in part by a grant from the National Cancer Institute (P30 CA047904; Dr. Robert L. Ferris-Principal Investigator). The microscope used in this study was funded by a shared instrumentation grant (1S100D019973-01; Simon Watkins-Principal Investigator).

References

Ambiye VR, Langade D, Dongre S, Aptikar P, Kulkami M, Dongre A, 2013 Clinical Evaluation of the Spermatogenic Activity of the Root Extract of Ashwagandha (*Withania sonmifera*) in Oligospermic Males: A Pilot Study. Evid. Based Complement. Alternat. Med 2013, 571420. [PubMed: 24371462]

Antony ML, Lee J, Hahm ER, Kim SH, Marcus AI, Kumari V, Ji X, Yang Z, Vowell CL, Wipf P, Uechi GT, Yates NA, Romero G, Sarkar SN, Singh SV, 2014 Growth arrest by the antitumor steroidal lactone withaferin A in human breast cancer cells is associated with down-regulation and covalent binding at cysteine 303 of β-tubulin. J. Biol. Chem 289, 1852–1865. [PubMed: 24297176]

Arnoult D, Grodet A, Lee YJ, Estaquier J, Blackstone C, 2005 Release of OPA1 during apoptosis participates in the rapid and complete release of cytochrome *c* and subsequent mitochondrial fragmentation. J. Biol. Chem 280, 35742–35750. [PubMed: 16115883]

Boland ML, Chourasia AH, Macleod KF, 2013 Mitochondrial dysfunction in cancer. Front. Oncol 3, 1–28. [PubMed: 23373009]

Brooks C, Dong Z, 2007 Regulation of mitochondrial morphological dynamics during apoptosis by Bcl-2 family proteins: a key in Bak? Cell Cycle 6, 3043–3047. [PubMed: 18073534]

Cassidy-Stone A, Chipuk JE, Ingerman E, Song C, Yoo C, Kuwana T, Kurth MJ, Shaw JT, Hinshaw JE, Green DR, Nunnari J, 2008 Chemical inhibition of the mitochondrial division dynamin reveals its role in Bax/Bak-dependent mitochondrial outer membrane permeabilization. Dev. Cell 14, 193–204. [PubMed: 18267088]

Cereghetti GM, Stangherlin A, Martins de Brito O., Chang CR, Blackstone C, Bernardi R, Scorrano L, 2008 Dephosphorylation by calcineurin regulates translocation of Drpl to mitochondria. Proc. Natl. Acad. Sci. U. S. A 105, 15803–15808. [PubMed: 18838687]

Chandrasekhar K, Kapoor J, Anishetty S, 2012 A prospective, randomized double-blind, placebo-controlled study of safety and efficacy of a high-concentration full-spectrum extract of *Ashwagcmdha* root in reducing stress and anxiety in adults. Indian J. Psychol. Med 34, 255–262. [PubMed: 23439798]

Cho B, Choi SY, Cho HM, Kim HJ, Sun W, 2013 Physiological and pathological significance of dynamin-related protein 1 (Drpl)-dependent mitochondrial fission in the nervous system. Exp. Neurobiol 22, 149–157. [PubMed: 24167410]

Chirumamilla CS, Pérez-Novo C, Van Ostade X, Vanden Berghe W, 2017 Molecular insights into cancer therapeutic effects of the dietary medicinal phytochemical withaferin A. Proc. Nutr. Soc 76, 96–105. [PubMed: 28162105]

Corrado M, Scorrano L, Campello S, 2012 Mitochondrial dynamics in cancer and neurodegenerative and neuroinflammatory diseases. Int. J. Cell Biol 2012, 729290. [PubMed: 22792111]

Estaquier J, Arnoult D, 2007 Inhibiting Drpl-mediated mitochondrial fission selectively prevents the release of cytochrome c during apoptosis. Cell Death Differ 14, 1086–1094. [PubMed: 17332775]

Grandemange S, Herzig S, Martinou JC, 2009 Mitochondrial dynamics and cancer. Semin. Cancer Biol 19, 50–56. [PubMed: 19138741]

Gu M, Yu Y, Gunaherath GM, Gunatilaka AA, Li D, Sun D, 2014 Structure-activity relationship (SAR) of withanolides to inhibit Hsp90 for its activity in pancreatic cancer cells. Invest. New Drugs 32, 68–74. [PubMed: 23887853]

Hahm ER, Lee J, Huang Y, Singh SV, 2011a Withaferin A suppresses estrogen receptor-α expression in human breast cancer cells. Mol. Carcinog 50, 614–624. [PubMed: 21432907]

Hahm ER, Lee J, Kim SH, Sehrawat A, Arlotti JA, Shiva SS, Bhargava R, Singh SV, 2013 Metabolic alterations in mammary cancer prevention by withaferin A in a clinically relevant mouse model. J. Natl. Cancer Inst 105, 1111–1122. [PubMed: 23821767]

Hahm ER, Lee J, Singh SV, 2014 Role of mitogen-activated protein kinases and Mcl-1 in apoptosis induction by withaferin A in human breast cancer cells. Mol. Carcinog 53, 907–916. [PubMed: 24019090]

Hahm ER, Moura MB, Kelley EE, Van Houten B, Shiva S, Singh SV, 2011b Withaferin A-induced apoptosis in human breast cancer cells is mediated by reactive oxygen species. PLoS One 6, e23354. [PubMed: 21853114]

Inoue-Yamauchi A, Oda H, 2012 Depletion of mitochondrial fission factor DRP1 causes increased apoptosis in human colon cancer cells. Biochem. Biophys. Res. Commun 421, 81–85. [PubMed: 22487795]

Jaradat NA, Al-Ramahi R, Zaid AN, Ayesh OI, Eid AM, 2016 Ethnopharmacological survey of herbal remedies used for treatment of various types of cancer and their methods of preparations in the West Bank-Palestine. BMC Complement. Altern. Med 16, 93. [PubMed: 26955822]

Jiang X, Jiang H, Shen Z, Wang X, 2014 Activation of mitochondrial protease OMA1 by Bax and Bak promotes cytochrome c release during apoptosis. Proc. Natl. Acad. Sci. U. S. A 111, 14782–14787. [PubMed: 25275009]

Kim SH, Singh SV, 2014 Mammary cancer chemoprevention by withaferin A is accompanied by *in vivo* suppression of self-renewal of cancer stem cells. Cancer Prev. Res. (Phila.) 7, 738–747. [PubMed: 24824039]

Lee J, Hahm ER, Marcus AI, Singh SV, 2015 Withaferin A inhibits experimental epithelial-mesenchymal transition in MCF-10A cells and suppresses vimentin protein level in vivo in breast tumors. Mol. Carcinog 54, 417–429. [PubMed: 24293234]

Lee J, Hahm ER, Singh SV, 2010 Withaferin A inhibits activation of signal transducer and activator of transcription 3 in human breast cancer cells. Carcinogenesis 31, 1991–1998. [PubMed: 20724373]

Lee YJ, Jeong SY, Karbowski M, Smith CL, Youle RJ, 2004 Roles of the mammalian mitochondrial fission and fusion mediators Fis1, Drp1, and Opa1 in apoptosis. Mol. Biol. Cell 15, 5001–5011. [PubMed: 15356267]

Lima AR, Santos L, Correia M, Soares P, Sobrinho-Simoes M, Melo M, Máximo V, 2018 Dynamin-Related Protein 1 at the Crossroads of Cancer. Genes (Basel) 9, 115.

MacVicar T, Langer T, 2016 OPA1 processing in cell death and disease - the long and short of it. J. Cell Sci 129, 2297–2306. [PubMed: 27189080]

Maycotte P, Marín-Hernández A, Goyri-Aguirre M, Anaya-Ruiz M, Reyes-Leyva J, Cortés-Hernández P, 2017 Mitochondrial dynamics and cancer. Tumour Biol 39, 1–16.

Mirjalili MH, Moyano E, Bonfill M, Cusido RM, Palazon J, 2009 Steroidal lactones from *Withcmia sonmifera*, an ancient plant for novel medicine. Molecules 14, 2373–2393. [PubMed: 19633611]

Olichon A, Baricault L, Gas N, Guillou E, Valette A, Belenguer P, Lenaers G, 2003 Loss of OPA1 perturbates the mitochondrial inner membrane structure and integrity, leading to cytochrome *c* release and apoptosis. J. Biol. Chem 278, 7743–7746. [PubMed: 12509422]

Palliyaguru DL, Singh SV, Kensler TW, 2016 *Withania sonmifera*: From prevention to treatment of cancer. Mol. Nutr. Food Res, 60, 1342–1353. [PubMed: 26718910]

Pham TD, Pham PQ, Li J, Letai AG, Wallace DC, Burke PJ, 2016 Cristae remodeling causes acidification detected by integrated graphene sensor during mitochondrial outer membrane permeabilization. Sci. Rep 6, 35907. [PubMed: 27786282]

Rehman J, Zhang HJ, Toth PT, Zhang Y, Marsboom G, Hong Z, Salgia R, Husain AN, Wietholt C, Archer SL, 2012 Inhibition of mitochondrial fission prevents cell cycle progression in lung cancer. FASEB J 26, 2175–2186. [PubMed: 22321727]

Samanta SK, Sehrawat A, Kim SH, Hahm ER, Shuai Y, Roy R, Pore SK, Singh KB, Christner SM, Beumer JH, Davidson NE, Singh SV, 2016 Disease subtype-independent biomarkers of breast cancer chemoprevention by the ayurvedic medicine phytochemical withaferin A. J. Natl. Cancer Inst 109, djw293.

Sehrawat A, Croix CS, Baty CJ, Watkins S, Tailor D, Singh RP, Singh SY, 2016 Inhibition of mitochondrial fusion is an early and critical event in breast cancer cell apoptosis by dietary chemopreventative benzyl isothiocyanate. Mitochondrion 30, 67–77. [PubMed: 27374852]

Sehrawat A, Roy R, Pore SK, Hahm ER, Samanta SK, Singh KB, Kim SH, Singh K, Singh SV, 2017 Mitochondrial dysfunction in cancer chemoprevention by phytochemicals from dietary and medicinal plants. Semin. Cancer Biol 47, 147–153. [PubMed: 27867044]

Sharma AK, Basu I, Singh S, 2018 Efficacy and Safety of Ashwagandha Root Extract in Subclinical Hypothyroid Patients: A Double-Blind, Randomized Placebo-Controlled Trial. J. Altern. Complement. Med 24, 243–248. [PubMed: 28829155]

Siegel RL, Miller KD, Jemal A, 2018 Cancer statistics, 2018. CA Cancer J. Clin 68, 7–30. [PubMed: 29313949]

Signes A, Fernandez-Vizarra E 2018 Assembly of mammalian oxidative phosphorylation complexes I-V and supercomplexes. Essays Biochem 62, 255–270. [PubMed: 30030361]

Stan SD, Zeng Y, Singh SV, 2008 Ayurvedic medicine constituent withaferin a causes G2 and M phase cell cycle arrest in human breast cancer cells. Nutr. Cancer 60, 51–60. [PubMed: 19003581]

Suen DF, Norris KL, Youle RJ, 2008 Mitochondrial dynamics and apoptosis. Genes Dev 22, 1577–1590. [PubMed: 18559474]

Thaiparambil JT, Bender L, Ganesh T, Kline E, Patel P, Liu Y, Tighiouart M, Vertino PM, Harvey RD, Garcia A, Marcus AI, 2011 Withaferin A inhibits breast cancer invasion and metastasis at sub-cytotoxic doses by inducing vimentin disassembly and serine 56 phosphorylation. Int. J. Cancer 129, 2744–2755. [PubMed: 21538350]

Vyas AR, Singh SV, 2014 Molecular targets and mechanisms of cancer prevention and treatment by withaferin A, a naturally occurring steroidal lactone. AAPS J 16, 1–10. [PubMed: 24046237]

Woods LC, Berbusse GW, Naylor K, 2016 Microtubules are essential for mitochondrial dynamics-fission, fusion, and motility–in *Dictyostelium discoideam*. Front. Cell Dev. Biol 4, 19. [PubMed: 27047941]

Xiao D, Srivastava SK, Lew KL, Zeng Y, Hershberger P, Johnson CS, Trump DL, Singh SV, 2003 Allyl isothiocyanate, a constituent of cruciferous vegetables, inhibits proliferation of human

prostate cancer cells by causing G2/M arrest and inducing apoptosis. Carcinogenesis 24, 891–897. [PubMed: 12771033]

Zhang H, Samadi AK, Cohen MS, Timmermann BN, 2012 Antiproliferative withanolides from the Solanaceae: A structure-activity study. Pure Appl. Chem 84, 1353–1367. [PubMed: 24098060]

Zhao J, Zhang J, Yu M, Xie Y, Huang Y, Wolff DW, Abel PW, Tu Y, 2013 Mitochondrial dynamics regulates migration and invasion of breast cancer cells. Oncogene 32, 4814–4824. [PubMed: 23128392]

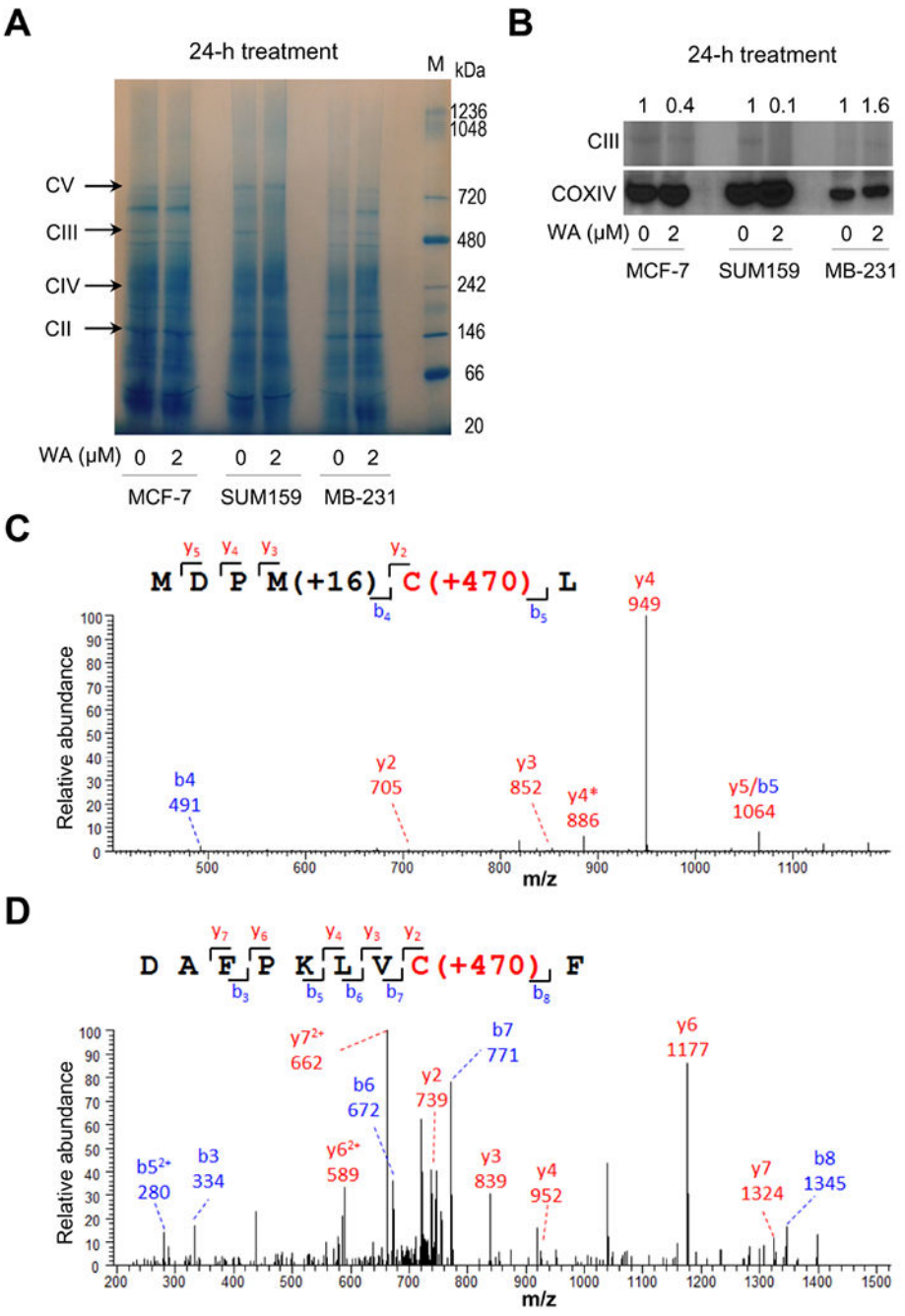

Fig. 1.

Withaferin A (WA) altered mitochondrial complex III in human breast cancer cells. **(A)** Blue native polyacrylamide gel electrophoresis showing mitochondrial complexes in MCF-7, SUM159, and MDA-MB-231 (MB-231) human breast cancer cells treated with DMSO or 2 μM of WA for 24 hours. **(B)** Quantification of complex III and COXIV in control and WA-treated MCF-7, SUM159, and MDA-MB-231 (MB-231) cells exposed to DMSO or 2 μM of WA for 24 hours. Tandem mass spectrum for identified WA modified glutathione S-transferase peptides **(C)** MDPMCL and **(D)** DAFPKLVCF from recombinant glutathione S-

transferase-tagged UQCRFS1 protein incubated with WA. The symbol * indicates fragment with neutral loss of oxidized methionine.

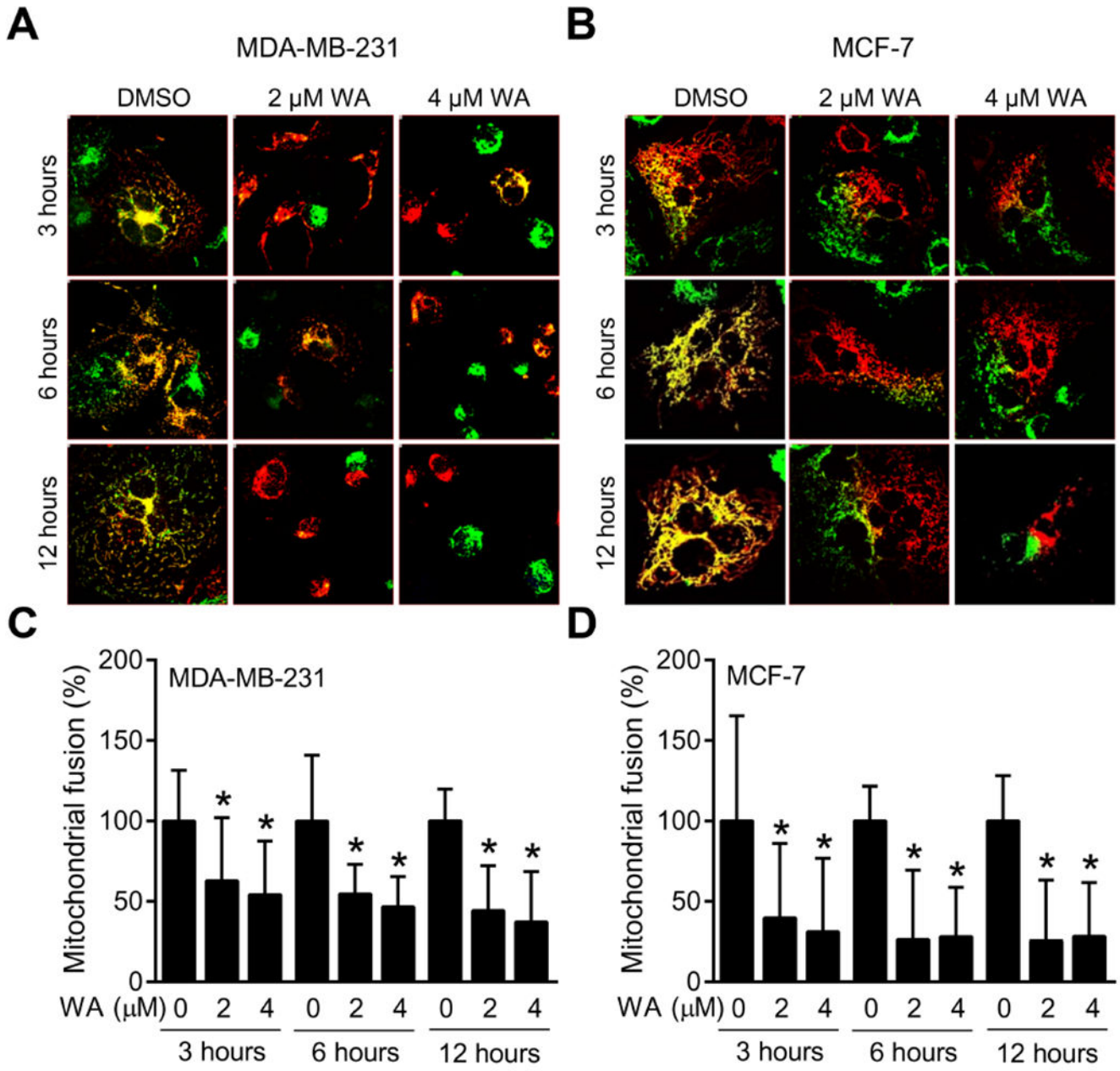

Fig. 2.

Withaferin A (WA) treatment inhibits PEG-induced mitochondrial fusion in human breast cancer cells. MDA-MB-231 and MCF-7 cells stably expressing mito-DsRed2 or mito-GFP were used for PEG fusion assay. Representative images from one of the two independent experiments are shown for MDA-MB-231 (**A,** 40× objective magnification) and MCF-7 (**B,** 60× objective magnification) cells after 3-, 6- or 12-hour treatment with DMSO or the indicated doses of WA. Quantification of WA-mediated inhibition of PEG-induced mitochondrial fusion relative to DMSO-treated control in MDA-MB-231 **(C)** and MCF-7 **(D)** cells. Percentage of co-localized fluorescence signal was determined in randomly selected fields with the use of Nikon (NIS) Elements software. Combined results from two

independent experiments are shown as mean ± SD (n = 20). *Significant ($P < 0.05$) compared with control by one-way analysis of variance (ANOVA) followed by Dunnett's adjustment.

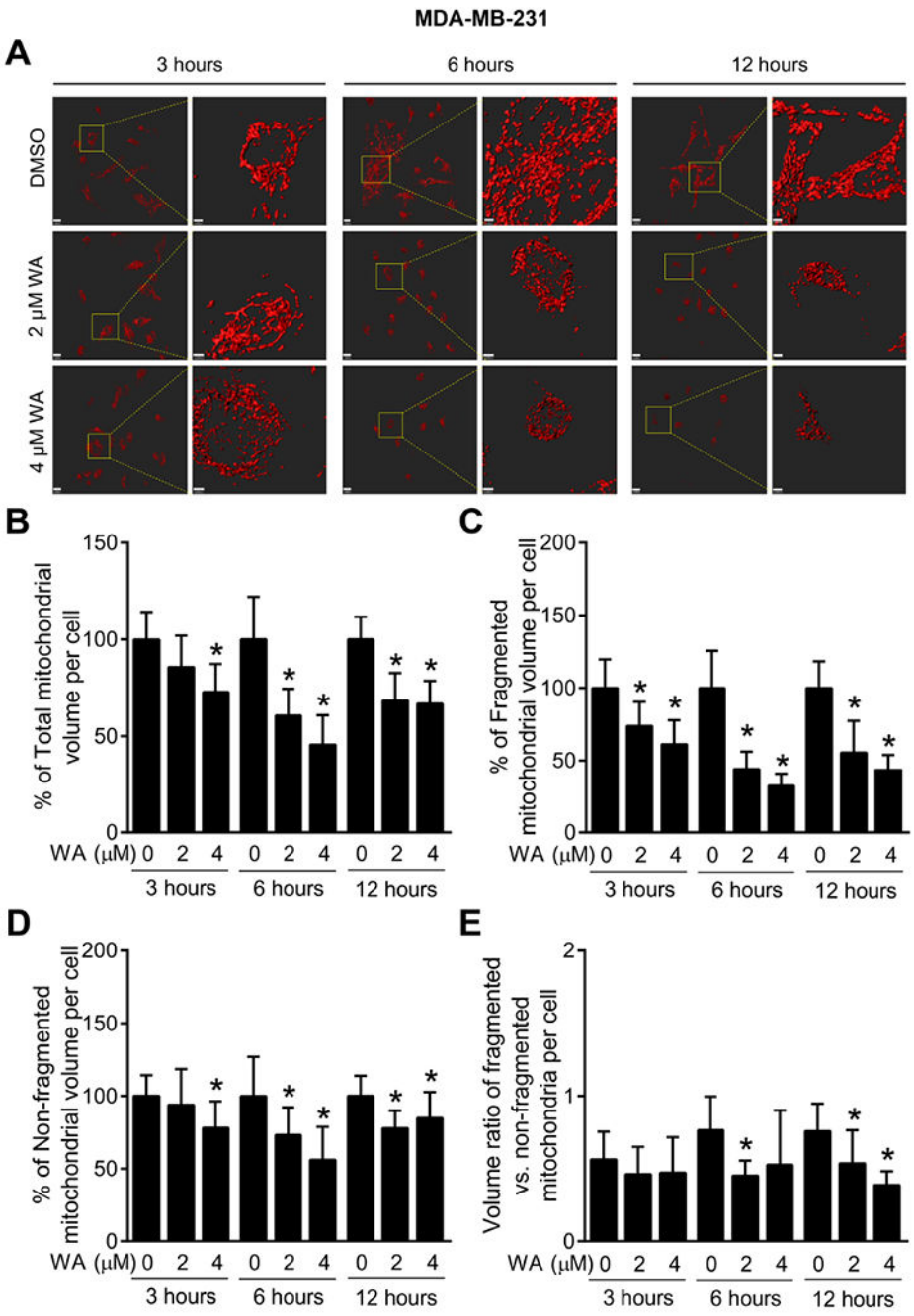

Fig. 3.

WA treatment causes a loss in mitochondrial volume in MDA-MB-231 human breast cancer cells. **(A)** Representative images of three-dimensional surface reconstructions using Imaris 8 software in mito-DsRed2 expressing MDA-MB-231 cells (scale bar, 15 μm) after 3-, 6- or 12-hour treatment with DMSO (control) or the indicated doses of WA. Enlarged images are shown in the right panel for each set (scale bar, 3 μm). Confocal microscopic images were collected as a Z-series for each position, using a Nikon A1 microscope (60× objective magnification). Images were deconvoluted using the 3D Landwebser deconvolution

capabilities of Nikon Elements and imported into Imaris software. Mitochondrial volume, surface area, and sphericity were calculated using Imaris software. Quantification of percentage of **(B)** total mitochondrial volume per cell, **(C)** fragmented mitochondrial volume per cell, **(D)** non-fragmented mitochondrial volume per cell, and **(E)** ratio of the fragmented *versus* non-fragmented mitochondrial volume in mito-DsRed2 expressing MDA-MB-231 cells after 3-, 6- or 12-hour treatment with DMSO or the indicated doses of WA. Mitochondrial fragmentation was assessed using sphericity parameter for small mitochondrial fragments, with an arbitrary threshold of sphericity < 0.4 to differentiate the fragmented mitochondria from total mitochondrial volume. Combined results from two independent experiments are shown as mean ± SD (n = 11). *Significant ($P < 0.05$) compared with control by one-way ANOVA followed by Dunnett's adjustment.

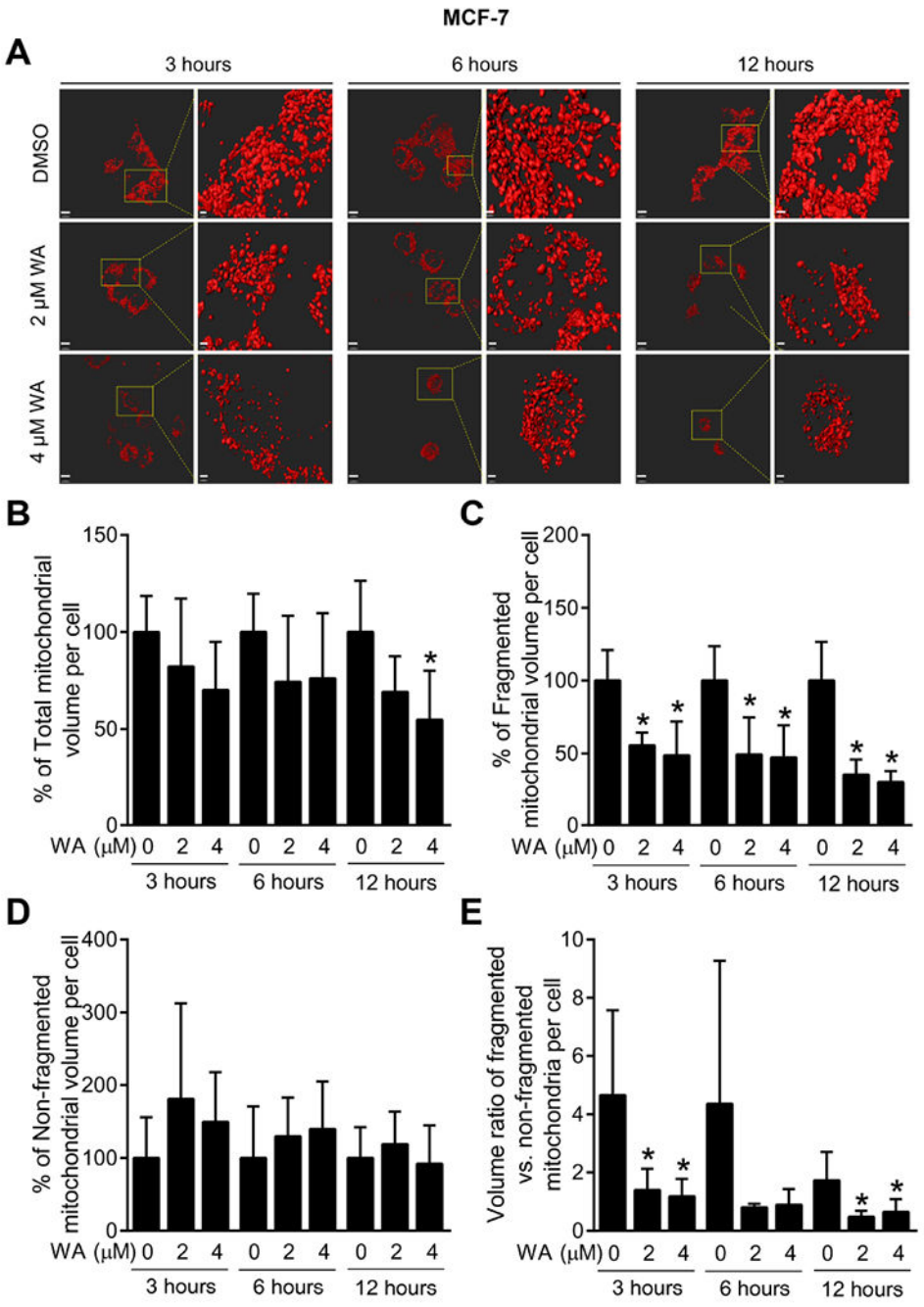

Fig. 4.

WA-caused loss in mitochondrial volume in MCF-7 human breast cancer cells. **(A)** Representative images of three-dimensional surface reconstructions using Imaris 8 software in mito-DsRed2 expressing MCF-7 cells (scale bar, 15 μm) after 3-, 6- or 12-hour treatment with DMSO (control) or the indicated doses of WA. Enlarged images are shown in the right panel for each set (scale bar, 3 pm). Confocal microscopic images were collected as a Z-series for each position, using a Nikon A1 microscope (60× objective magnification). Image analysis was done as described for Fig. 3. Quantification of percentage of **(B)** total

mitochondrial volume per cell, **(C)** fragmented mitochondrial volume per cell, **(D)** non-fragmented mitochondrial volume per cell, and **(E)** ratio of the fragmented *versus* non-fragmented mitochondrial volume in mito-DsRed2 expressing MCF-7 cells after 3-, 6- or 12-hour treatment with DMSO or the indicated doses of WA. Results shown are mean ± SD (n = 5). *Significant ($P < 0.05$) compared with control by one-way ANOVA with Dunnett's adjustment.

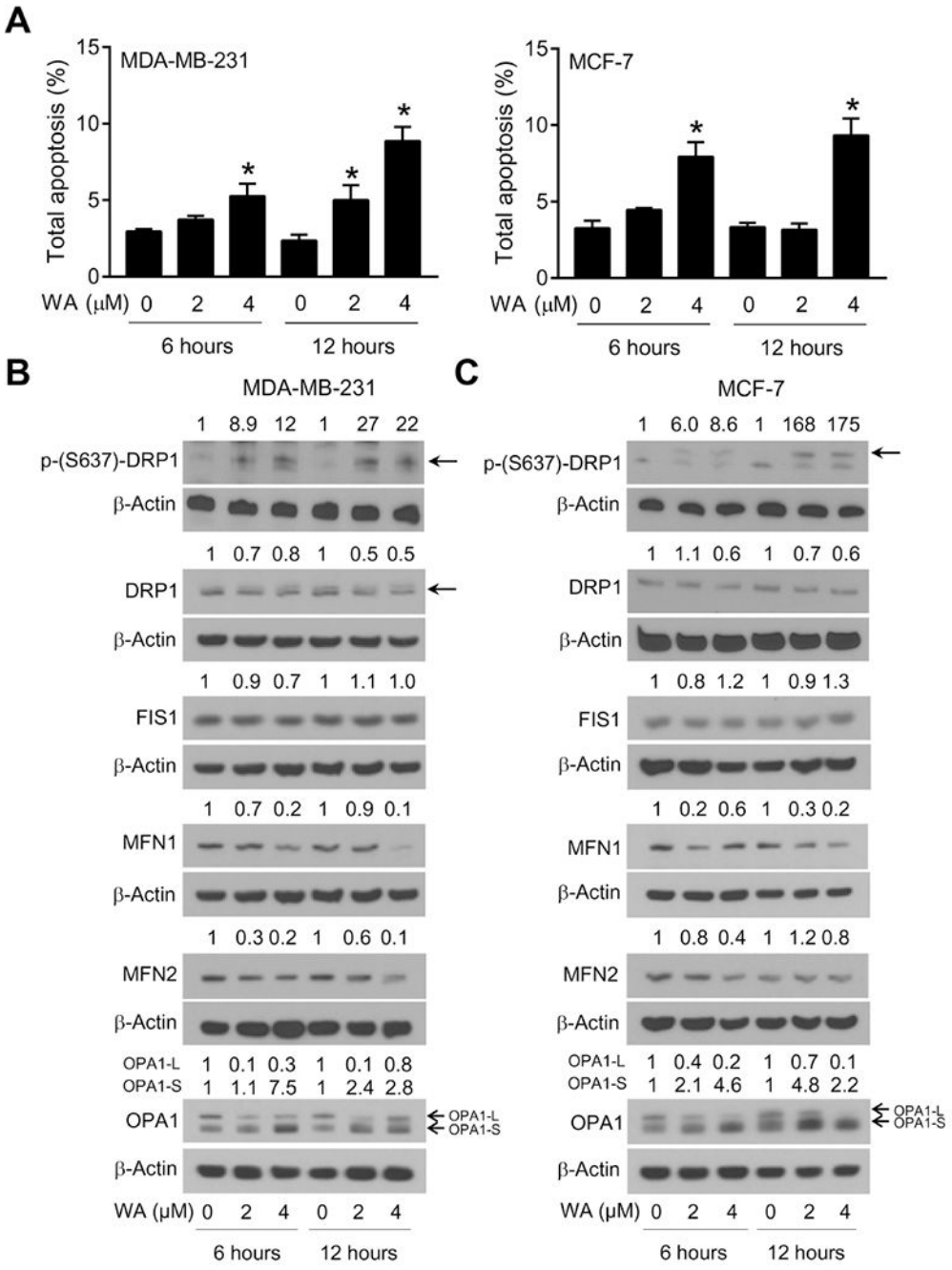

Fig. 5.

Withaferin A (WA)-mediated apoptosis was associated with alterations in expression of proteins responsible for mitochondrial fusion and fission in human breast cancer cells. **(A)** Quantification of percentage of total apoptosis in MDA-MB-231 and MCF-7 cells treated with DMSO or the indicated doses of WA for the specified time periods. Results shown are mean ± SD (n = 3). *Significant ($P < 0.05$) compared with respective control by one-way ANOVA followed by Dunnett's adjustment. Consistent results were obtained from independent experiments. Western blotting for phospho-DRPl (S637), total DRP1, FIS1,

MFN1, MFN2, and 0PA1-L and OPA1-S proteins using lysates from **(B)** MDA-MB-231 and **(C)** MCF-7 cells after 6- or 12-hour treatment with DMSO or the indicated doses of WA. Numbers on top of the immunoreactive bands represent changes in protein levels relative to corresponding DMSO-treated control. Arrows indicate correct band for the proteins. Results were comparable in replicate experiments.

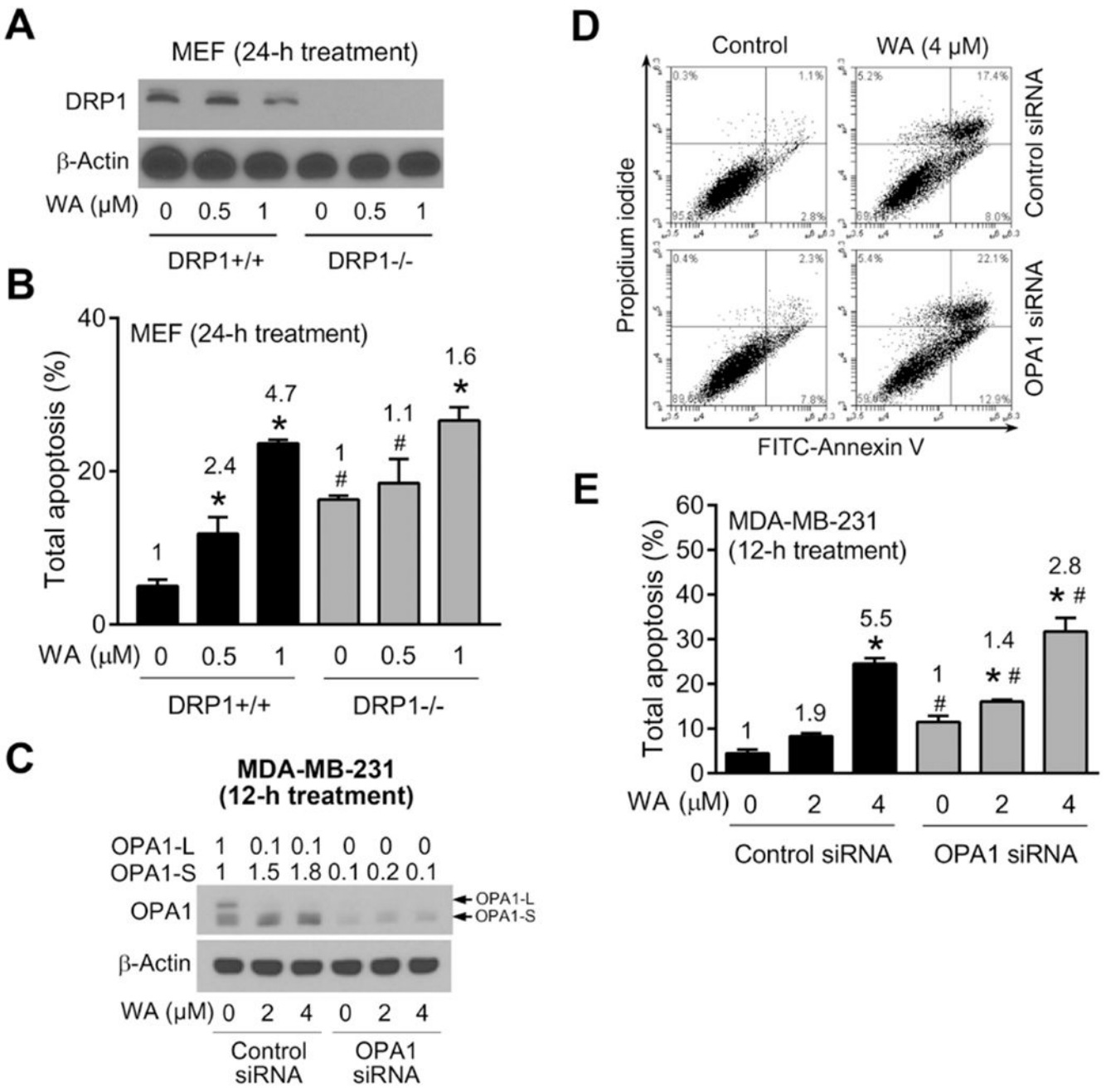

Fig. 6.

Effect of DRP1 deficiency and OPA1 knockdown on WA-induced apoptosis. **(A)** Immunoblotting for DRP1 using lysates from DRP1+/+ and DRP1−/− MEF treated for 24 hours with DMSO or the indicated doses of WA. **(B)** Quantification of % total apoptosis (early + late apoptosis) in DRP1+/+ and DRP1−/− MEF treated for 24 hours with DMSO or the indicated doses of WA. Results shown are mean ± SD (n = 3). Significant ($P < 0.05$) compared with *Respective DMSO-treated control, and #between DRP1+/+ and DRP1−/− MEF at the same treatment by one-way ANOVA followed by Bonferroni's comparisons test. The numbers in the bar graph represent fold increase in apoptosis relative to corresponding

DMSO-treated control. **(C)** Immunoblotting for OPA1-L and OPA-S using lysates from MDA-MB-231 cells transiently transfected with 100 nM control siRNA or 100 nM OPA1-targeted siRNA for 24 hours and then treated for 12 hours with DMSO or the indicated doses of WA. Arrows indicate correct band for the proteins. **(D)** Representative flow histograms for MDA-MB-231 cells transiently transfected with control siRNA or OPA1-targeted siRNA for 24 hours and treated for 12 hours with DMSO or 4 μM WA. **(E)** Quantification of % total apoptosis (early + late apoptosis in MDA-MB-231 cells transiently transfected with control siRNA or OPA1-targeted siRNA for 24 hours and then treated for 12 hours with DMSO or the indicated doses of WA. Results shown are mean ± SD (n = 3). Significant ($P < 0.05$) compared with *Respective DMSO-treated control, and #between control siRNA and OPA1 siRNA by one-way ANOVA followed by Bonferroni's comparisons test. The numbers in the bar graph represent fold increase in apoptosis relative to corresponding DMSO-treated control. Results were comparable in replicate experiments.